Inorganic Chemistry

Article

pubs.acs.org/IC

Morphotropy and Temperature-Driven Polymorphism in $A_2Th(AsO_4)_2$ (A = Li, Na, K, Rb, Cs) Series

Na Yu,[†] Vladislav V. Klepov,[†,‡] Giuseppe Modolo,[†] Dirk Bosbach,[†] Evgeny V. Suleimanov,[§] Thorsten M. Gesing,[∥] Lars Robben,[∥] and Evgeny V. Alekseev*[,†,⊥]

[†]Forschungszentrum Jülich GmbH, Institute for Energy and Climate Research (IEK-6), 52428 Jülich, Germany

[‡]Department of Chemistry, Samara State University, 443011 Samara, Russia

[§]Department of Chemistry, Lobachevsky State University of Nizhny Novgorod, 603950 Nizhny Novgorod, Russia

[∥]Chemische Kristallographie fester Stoffe, Institut für Anorganische Chemie, Universität Bremen, Leobener Straße, D-28359 Bremen, Germany

[⊥]Institut für Kristallographie, RWTH Aachen University, 52066 Aachen, Germany

Supporting Information

ABSTRACT: A new alkaline thorium arsenate family was obtained and systematically investigated. The structures of $A_2Th(AsO_4)_2$ (A = Li, Na, K, Rb, Cs) were determined from single crystal X-ray diffraction data. $Li_2Th(AsO_4)_2$ and either isostructural $K_2Th(AsO_4)_2$ and $Rb_2Th(AsO_4)_2$ crystallize in the monoclinic crystal system. $Na_2Th(AsO_4)_2$ and $Cs_2Th(AsO_4)_2$ crystallize in the orthorhombic and tetragonal crystal systems, respectively. $Li_2Th(AsO_4)_2$ consists of $[Th(AsO_4)_2]^{2-}$ layers with Li atoms in the interlayer space. The rest of the compounds are based on 3D frameworks. Differences in local environments of ThO_8 coordination polyhedra are described in relation to the symmetry. Despite different local environments of ThO_8 coordination polyhedra and different structural symmetry, underlying nets of $A_2Th(AsO_4)_2$ (A = Na, K, Rb, Cs) were shown to be the same. Single-crystal and powder Raman spectra were measured, and bands are assigned. DSC measurements showed phase transitions in $K_2Th(AsO_4)_2$ and $Rb_2Th(AsO_4)_2$, which were studied using high-temperature powder X-ray diffraction (HT-PXRD). The data of HT-PXRD demonstrates two high-temperature polymorphic modification of $K_2Th(AsO_4)_2$ and only one for the isotypic $Rb_2Th(AsO_4)_2$. The phase transitions in both K and Rb phases are reversible.

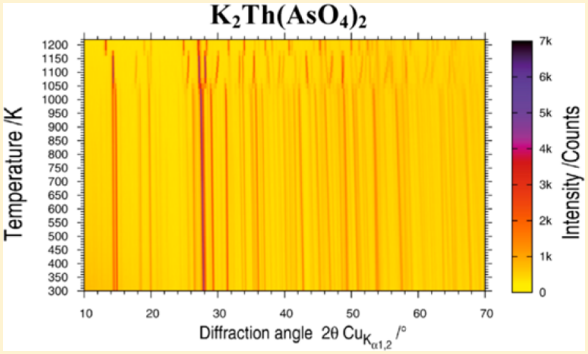

1. INTRODUCTION

Actinide inorganic chemistry is of great importance both from a fundamental and an applied point of view. The main feature of the actinides in comparison to other elements is the presence of 5f electrons that leads to a variety of oxidation states (from +2 to +8[1−3]) of light actinides and, therefore, diversity of their chemical properties. Synthetic conditions have a strong influence on phase formation in actinide chemistry.[4−6] For example, there are two very stable oxidation states for uranium, namely, +4 and +6. U(IV) compounds are usually obtained in reductive media and U(IV) in the structures of such compounds plays the role of tetravalent cation. In contrast, U(VI) shows a strong tendency of linear divalent uranyl cation UO_2^{2+} formation, which, to a wide extend, determines the crystal chemical properties of U(VI). Compared to U(IV), only minor research has been carried out on the investigation of Np(IV)- and Pu(IV)-containing phases due to higher radioactivity. Much less radioactive Th(IV) has a quite similar coordination chemistry compared to Np(IV) and Pu(IV)[7−10] as well as with U(IV), which makes Th(IV) highly suitable to model the behavior of those elements.

Actinide phosphates and polyphosphates attract significant interest as they show both structural and chemical diversity as well as promising properties. An example of the latter is thorium phosphate diphosphate $Th_4(PO_4)_4(P_2O_7)$, which is proposed as a host matrix for large amounts of uranium and plutonium.[11−15] The structural diversity of Th and U phosphates can be illustrated by a number of works published during the past decade.[16−22] Recently, a number of research focused on alkaline thorium phosphates have been performed.[23−26] Nevertheless, data on thorium arsenates are not so plentiful, although arsenates can serve as a comparative element due to similarities between arsenate and phosphate ions. For example, the crystal structure of α-Li$[(UO_2)(AsO_4)]$ is isomorphic to α-Li$[(UO_2)(PO_4)]$,[18] and $Li(UO_2)_4(AsO_4)_3$[27] is topologically identical to the structure of $Li(UO_2)_4(PO_4)_3$.[17] Despite this, due to the anions' size difference, it is not always true that phosphates and arsenates form compounds with similar structures and/or stoichiometry at the similar synthetic conditions. In this respect, we carried out a

Received: July 29, 2014
Published: October 2, 2014

   dx.doi.org/10.1021/ic5018246 | Inorg. Chem. 2014, 53, 11231−11241

Table 1. Crystallographic Data for $A_2Th(AsO_4)_2$ (A = Li, Na, K, Rb, Cs) Collected at 293(2) K

compound	$Li_2Th(AsO_4)_2$	$Na_2Th(AsO_4)_2$	$K_2Th(AsO_4)_2$	$Rb_2Th(AsO_4)_2$	$Cs_2Th(AsO_4)_2$
space group	$P\,2_1/c$	$F\,ddd$	$P\,2_1/n$	$P\,2_1/n$	$I\,4_1/amd$
a /Å	9.1841(3)	7.0425(3)	7.7576(3)	8.0380(8)	7.3205(5)
b /Å	13.7468(4)	12.3268(4)	11.3648(3)	11.4510(9)	a
c /Å	5.63541(17)	18.2185(5)	9.4826(4)	9.6692(10)	18.623(2)
β /°	106.503(3)	90.00	110.756(5)	111.137(12)	90.00
V /Å^3	682.17(3)	1581.58(10)	781.75(5)	830.11(14)	998.0(1)
D_{calc} /g/cm^3	5.08	4.669	4.997	5.448	5.163
Z	4	8	4	4	4
λ /Å	0.71073	0.71073	0.71073	0.71073	0.71073
$F(000)$	904	1936	1032	1176	1320
$R1$	0.0384	0.0144	0.0317	0.0346	0.0384
$wR2$	0.1084	0.0273	0.0935	0.0709	0.1117

$R(F) = \Sigma||F_o| - |F_c||/\Sigma|F_o|$. $wR(F_o^2) = [\Sigma w(F_o^2 - F_c^2)^2/\Sigma w(F_o^2)^2]^{1/2}$.

systematical investigation of the $A^I - As_2O_5 - ThO_2$ (A^I = Li, Na, K, Rb, Cs) system. In this work, we report the details of synthesis, crystal structures, thermal behavior, polymorphism, and spectroscopic properties of the novel thorium arsenate series with $A_2Th(AsO_4)_2$ (A = Li, Na, K, Rb, Cs) general formula.

2. EXPERIMENTAL SECTION

Caution! Although ^{232}Th ($T_{1/2}$ = 1.4 × 10^{10} years) presents a low specific activity, standard precautions for handling radioactive materials should be followed when working with the quantities used in the syntheses that follow.

2.1. Chemicals. Thorium nitrate $Th(NO_3)_4{\cdot}5H_2O$ (Merck), lithium nitrate $LiNO_3$ (Alfa-Aesar, 99.9%), sodium nitrate $NaNO_3$ (Alfa-Aesar, 99.9%), potassium nitrate KNO_3 (Alfa-Aesar, 99.9%), rubidium nitrate $RbNO_3$ (Alfa-Aesar, 99.9%), cesium nitrate $CsNO_3$ (Alfa-Aesar, 99.9%), and ammonium dyhydrogen arsenate $NH_4H_2AsO_4$ (Alfa-Aesar, 98%) were used as received.

2.2. Syntheses of Single Crystals of Alkaline Thorium Arsenates. Single crystals of all titled compounds were obtained by high-temperature solid-state reactions. The chemicals of analytical reagent grade were used without any other further purification. The reactants were thoroughly ground together with their appropriate ratios and loaded into a platinum crucible. The molar ratio of $Th(NO_3)_4{\cdot}5H_2O/NH_4H_2AsO_4/ANO_3$ (A= Li/Na/K/Rb/Cs) was equal to 1:10:2/1:10:3/1:8:1/1:10:3/1:10:3, respectively. This reaction mixture was then placed into a program-controlled furnace (CARBOLITE CWF 1300) and heated to the designated temperature in 1 h. The crystals were grown after heating to the temperatures of 1273/1273/1123/1223/1273 K for A = Li/Na/K/Rb/Cs, respectively. Thereafter, the homogenized melt solution was cooled slowly (5 K/h) to the final crystallization temperature (673 K) and finally allowed to cool to room temperature by switching off the furnace. The reaction product consisted of colorless block-like crystals.

2.3. Pure Powder Samples Preparation. Pure phase powder of all 5 alkaline thorium arsenate compounds were prepared according to 1:2:2 stoichiometric ratios of $Th(NO_3)_4{\cdot}5H_2O$, $NH_4H_2AsO_4$, and ANO_3, where A = Li, Na, K, Rb, and Cs. Initial reagent mixtures were finely ground, heated up to 723 K with a heating rate of 300 K/h in air and kept at this temperature for 30 h. After cooling by switching off the furnace, the samples were ground and room-temperature powder X-ray diffraction was employed to check the purity of the polycrystalline samples. In case of inconsistency between experimental powder diffraction pattern and those calculated from single crystal X-ray diffraction, the samples were heated up to higher temperature until a pure phase powder samples was obtained. This procedure was performed with 50 K/step and 20 K/step temperature increase for the temperature ranges of 723−873 K and 873−1073 K, respectively. The final temperatures of pure phase formations are 1073, 993, 993, 1033, and 913 K for A = Li, Na, K, Rb, and Cs, respectively.

2.4. Single-Crystal X-ray Diffraction. Single crystal X-ray diffraction data were collected at room-temperature on a SuperNova (Agilent) diffractometer using MoKα radiation (λ = 0.71073 Å). Single crystals were mounted on a glass fiber with epoxy glue. The data were collected using a narrow-frame method with the ω-scan mode. The data were integrated using the CrysAlis^{Pro} program, and the intensities were corrected for Lorentz polarization and absorption attributable to the variation in the path length through the detector faceplate. Absorption correction based on the multiscan technique was applied. The structures were solved by direct method using SHELXS-97[28] and then refined by full-matrix least-squares refinement on F^2 with SHELXL-97 found in the software suite WinGX v1.80.05.[29] All of the structures were verified using the ADDSYM algorithm from the program PLATON, and no higher symmetries were found. Relevant crystallographic data and details of the experimental conditions for all five crystals are summarized in Table 1. All crystal chemical calculations were performed using the TOPOS software package (http://topos.samsu.ru).[30,31]

2.5. Powder X-ray Diffraction. Powder X-ray diffraction patterns were collected on a Bruker D4 Endeavor diffractometer, equipped with a Cu tube providing graphite monochromized Kα radiation (λ = 1.54187 Å) and a one-dimensional silicon strip LynxEye detector (Bruker), using a voltage equal 40 kV and an electric current equal 40 mA (1.6 kW). Data were recorded in the range of 2θ = 0° − 80° (total counting time = 10 s/step with the step width of = 0.02°). The aperture of the fixed divergence and receiving slit was set to 0.2 and 8.0 mm, respectively.

The temperature-dependent X-ray powder diffraction data were collected on a Panalytical MPD powder diffractometer using Bragg−Brentano geometry. The setup was equipped with a secondary Ni filter, Cu Kα radiation, an X'Celerator multi strip detector, and an Anton Paar HTK1200N heating chamber. The samples were placed as slurry of a sample−acetone mixture on a flat corundum holder resulting in small evaporation channels after drying which served for optimum space during thermal expansion of $K_2Th(AsO_4)_2$ and $Rb_2Th(AsO_4)_2$. Diffraction was carried out between 300 and 1220 K with a ramping slice of 20 K. Each diffraction pattern was recorded from 4° to 85° 2θ with a step size of 0.0167° and a 69.85 s/step total data collection time. The fundamental parameter approach, where the fundamental parameters were fitted against a LaB_6 standard material, was applied for the Rietveld refinement using "Diffrac^{Plus} Topas 4.2" software (Bruker AXS GmbH, Karlsruhe). For this purpose the starting atomic coordinates were taken from the single crystal diffraction quality data. The metric parameters further used for the description of the compounds were evaluated in that way in a very accurate manner.

2.6. Autocorrelation Analysis. For the autocorrelation analysis of the temperature-dependent X-ray diffraction data of $K_2Th(AsO_4)$ and $Rb_2Th(AsO_4)$ a suitable data range was selected (10° to 16° 2θ) and cut from the data sets. The selected data range was slightly denoised and the autocorrelations of the data segments were calculated according to the formula: $\mathrm{Corr}(f, f, \omega') = \int_{-\infty}^{\infty} f^*(\omega) f(\omega + \omega') d\omega$ (where f is the measured intensity at the 2θ value ω and ω' is the lag).[32] From this

dx.doi.org/10.1021/ic5018246 | Inorg. Chem. 2014, 53, 11231−11241

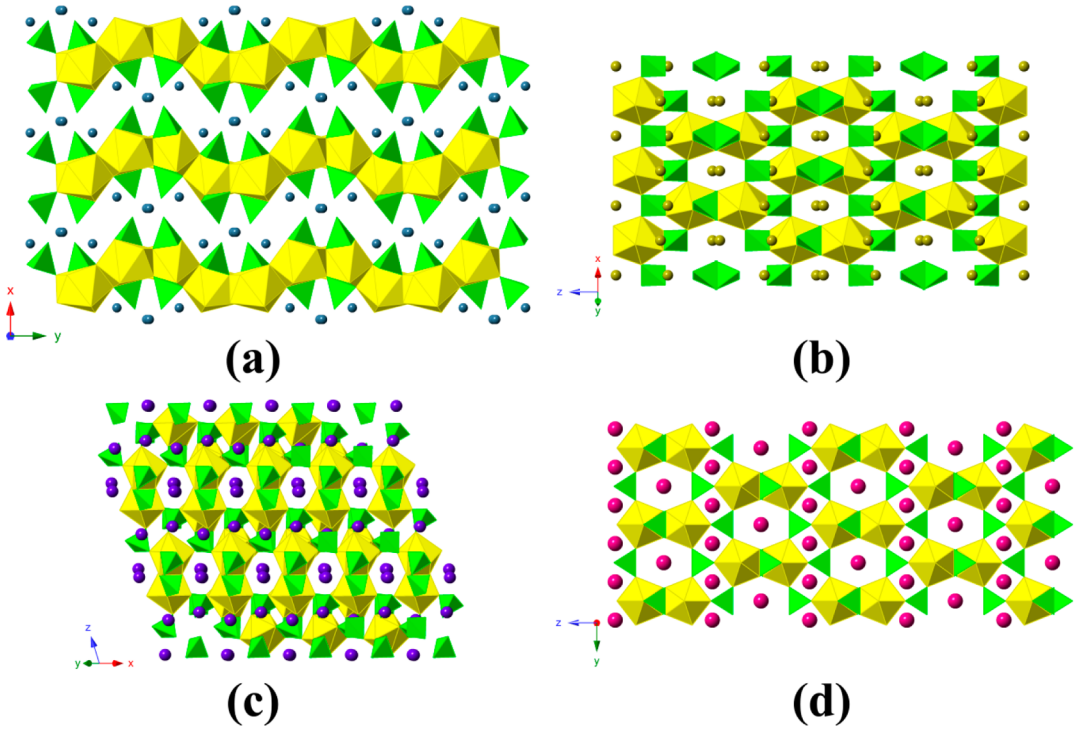

Figure 1. Polyhedral representation of the crystal structures of $Li_2Th(AsO_4)_2$ (a), $Na_2Th(AsO_4)_2$ (b), $K_2Th(AsO_4)_2$ (c), and $Cs_2Th(AsO_4)_2$ (d). $Rb_2Th(AsO_4)_2$ is isostructural with $K_2Th(AsO_4)_2$. Th and As polyhedra are shown in yellow and green, respectively, and alkaline atoms are represented as colored spheres.

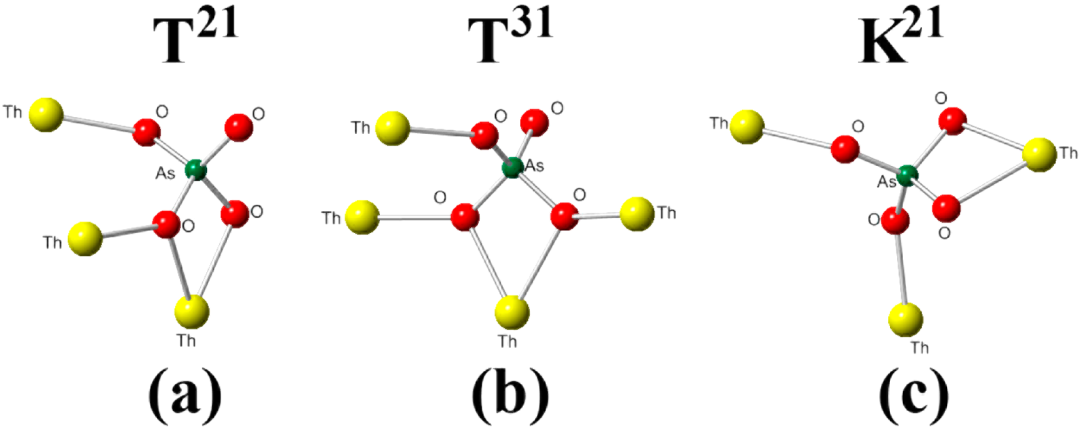

Figure 2. Coordination types of arsenate anions in the crystal structures of $A_2Th(AsO_4)_2$ (A = Li, Na, K, Rb, and Cs). T^{21} and T^{31} (a and b, respectively) coordination types in the structure of $Li_2Th(AsO_4)_2$ and K^{21} coordination type (c) in the structures of $A_2Th(AsO_4)_2$ (A = Na, K, Rb, and Cs).

autocorrelation data, the normalized autocorrelation for a lag of $\omega' = 1$ ($Corr_{Norm}(1)$) was chosen to characterize each single temperature data segment.

2.7. Element Analysis. The scanning electron microscopy (SEM) investigations were performed with the environmental scanning electron microscope FEI Quanta 200 F. The measurements were carried out in a low-vacuum mode at 0.6 mbar (30 kV, spot size 4, working distance 10 mm). When using this mode, sputtering of the samples with gold or carbon is not necessary, and artifacts are avoided. The powder and single crystals were prepared on adhesive carbon tabs. The microscope is equipped with an Apollo X Silicon Drift Detector (SDD) from EDAX. The results of elemental analysis are listed in Table S1 in Supporting Information.

2.8. TG-DSC Experiments. The thermal behavior of the dried powders was studied from room temperature to 1273 K by differential scanning calorimetry analysis (DSC) coupled with thermogravimetry (TG) in air at a heat rate of 10 K/min using a Netzsch STA 449C Jupiter apparatus. Each sample (20 mg) was loaded in a platinum crucible, which was closed with a platinum cover. During the measurements a constant air flow of 20−30 mL/min was applied.

2.9. Raman and IR Spectroscopy. Unpolarized Raman spectra were recorded with a Horiba LabRAM HR spectrometer using a Peltier cooled multichannel CCD detector. An objective with a 50× magnification was linked to the spectrometer allowing the analysis of samples as small as 2 μm in diameter. The sample was in the form of a polycrystalline powder. The incident radiation was produced by a HeNe laser (λ = 632.81 nm) at a power of 17 mW. The focal length of the spectrometer was 800 mm and a 1800 gr/mm grating was used. The spectral resolution was around 1 cm^{-1} with a slit of 100 μm. Spectra were recorded in the range of 50−1250 cm^{-1}. No significant photoluminescence was observed.

A Bruker Equinox spectrometer was used for the IR experiments, and the KBr pellet technique was applied for sample preparation. For this purpose, approximately 200 mg of desiccated KBr and 2 mg of each

dx.doi.org/10.1021/ic5018246 | Inorg. Chem. 2014, 53, 11231−11241

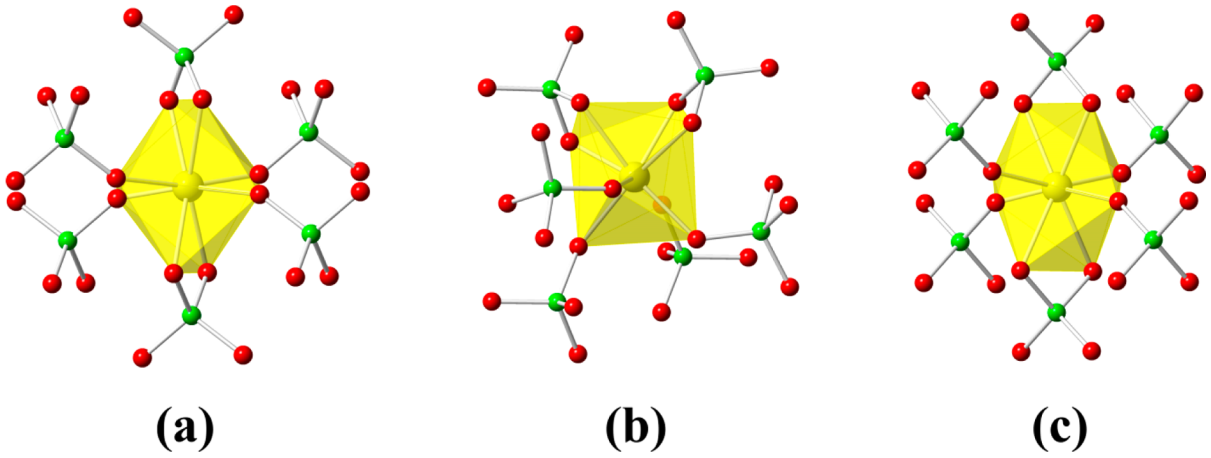

Figure 3. Second neighbor coordination of Th atoms in the crystal structures of $Na_2Th(AsO_4)_2$ (a), $A_2Th(AsO_4)_2$ (A = K, Rb) (b), and $Cs_2Th(AsO_4)_2$ (c). Th polyhedra are shown in yellow, As and O atoms are green and red, respectively.

sample were mixed carefully, and a pressure of 10 tons was applied and held constant for 3 min to prepare each pellet. The IR spectra were recorded in the range from 400 to 4000 cm^{-1}. A pure KBr pellet, which was prepared under the same experimental conditions, was used as a blank sample.

3. RESULTS AND DISCUSSION

3.1. Crystal Structure Description. *$Li_2Th(AsO_4)_2$.* $Li_2Th(AsO_4)_2$ crystallizes in the centrosymmetric monoclinic space group $P2_1/c$ (Table 1) and is based upon $[Th(AsO_4)_2]^{2-}$ 2D layers. The Li cations are located within the interlayer space (Figure 1a). Thorium atoms occupy a single crystallographic position and possess 9-fold oxygen coordination. The Th—O bond distances are in the range of 2.351(11)−2.582(9) Å. Two symmetrically independent arsenic atoms form AsO_4 tetrahedra with As—O bond lengths ranging from 1.650(10) Å to 1.718(10) Å. Arsenate anions can be assigned to T^{21} and T^{31} coordination types (Figure 2a,b) according to the classification given in the literature.[33,34] The uppercase of a given designation describes a number of donor oxygen atoms coordinating on Th atoms (M, B, T, K, etc. for mono-, bi-, tri-, tetradentate ligands[33]). The superscript numbers equal the amount of Th atoms connected through one, two, three, and so forth, donor O atoms, respectively. AsO_4 groups are coordinated to Th atoms only by three O atoms and have one terminal oxygen atom in the crystal structure of $Li_2Th(AsO_4)_2$ (Figure 2a,b). One can find that first two superscript positions are equal to the number of Th coordination polyhedra that share corner or edge with one arsenic polyhedron. Both ThO_9 and AsO_4 polyhedra form corrugated sheets parallel to (100) (Figure 1a).

There are two independent Li sites within the interlayer space that serve for a charge balancing and a connection of the layers into 3D assembly. Both Li atoms have 4-fold oxygen coordination with Li—O bond distances ranging from 1.91(3) Å to 2.34(4) Å.

$Na_2Th(AsO_4)_2$. $Na_2Th(AsO_4)_2$ crystallizes in an orthorhombic space group *F ddd* (Table 1) and based upon the 3D framework. The structure of $Na_2Th(AsO_4)_2$ (Figure 1b) shows significant differences compared to the chemically similar $Li_2Th(AsO_4)_2$. It contains only one symmetrically independent Th atom, which occupies a single site with D_2 local symmetry and is connected to eight O atoms with Th−O distances ranging from 2.3211(15) Å to 2.5453(14) Å. The arsenic atoms also occupy a single crystallographic position with C_2 site-symmetry. The As − O bond lengths in AsO_4 tetrahedra are equal to 1.6729(15) Å and 1.6872(15) Å. The arsenate anion is connected to three Th atoms with the mode shown in Figure 2c. The denticity of the arsenate-anions is four and can be designated with the letter K. Thus, the coordination type of arsenate-anions in the crystal structure of $Na_2Th(AsO_4)_2$ is K^{21}, which means that AsO_4 polyhedron shares two corners and one edge with three different ThO_8 polyhedra. It is noteworthy that the edge-sharing arsenate-anions are in *trans*-positions within the coordination environment of Th atoms (Figure 3a). The $[Th(AsO_4)_2]^{2-}$ framework contains chains of cages along {110} directions. The cages are occupied by Na atoms (Figure 1b) with the shortest Na—Na distances of 3.6061(4) Å.

$K_2Th(AsO_4)_2$ and $Rb_2Th(AsO_4)_2$. $K_2Th(AsO_4)_2$ and $Rb_2Th(AsO_4)_2$ are isostructural and crystallize in $P2_1/n$ space group. Both crystal structures are based on 3D framework that consists of corner- and edge-sharing ThO_8 and AsO_4 polyhedra (Figure 1c). Th atoms occupy a single crystallographic position and are bound to eight O atoms with bond distances in the ranges of 2.370(4)−2.520(4) Å and 2.363(6)−2.532(6) Å for A = K and Rb, respectively. Arsenate anions possess the same K^{21} coordination type as observed in $Na_2Th(AsO_4)_2$. As—O distances vary from 1.671(4) Å to 1.693(3) Å and 1.670(6) Å to 1.708(6) Å for A = K and Rb, respectively. The symmetry change, comparing to $Na_2Th(AsO_4)_2$, is raised from a stereometric change of the Th atom environment, which is expressed in the *cis*-positioning of the edge-sharing arsenate groups (Figure 3b). The chains of cages similar to those in $Na_2Th(AsO_4)_2$ are also existing in the structures of $K_2Th(AsO_4)_2$ and $Rb_2Th(AsO_4)_2$. The potassium and rubidium atoms reside in these cages with shortest interatomic d(A−A) distances in ranges of 3.51−3.62 Å and 3.54−3.68 Å for A = K and Rb, respectively.

$Cs_2Th(AsO_4)_2$. $Cs_2Th(AsO_4)_2$ crystallizes in the tetragonal space group $I4_1/amd$, which represents the highest symmetry of the series discussed here. It is a 3D framework based upon 8-fold-coordinated Th atoms surrounded by arsenate anions (Figure 1d). The Th−O and As−O bond distances are in the ranges of 2.355(10)−2.535(10) Å and 1.676(10)−1.686(10) Å, respectively. The crystal structure of $Cs_2Th(AsO_4)_2$ contains arsenate-anions with K^{21} coordination type, and the Th atoms are coordinated by bidentate arsenate groups in *trans*-positions. Generally, the structure of $Cs_2Th(AsO_4)_2$ shows more similarities to the crystal structure of $Na_2Th(AsO_4)_2$ than with those of $A_2Th(AsO_4)_2$ (A = K, Rb). Therefore, the lower

dx.doi.org/10.1021/ic5018246 | *Inorg. Chem.* 2014, 53, 11231−11241

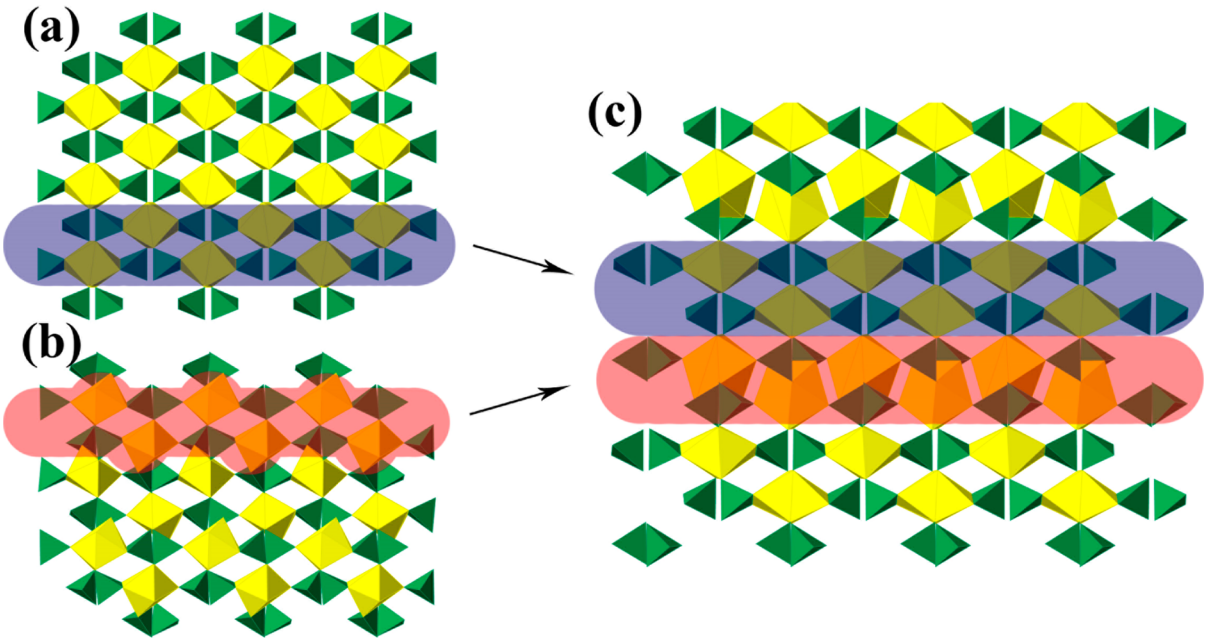

Figure 4. Comparison of the crystal structures of $Na_2Th(PO_4)_2$ (c) and $A_2Th(AsO_4)_2$ (A = Na, K) (a, b, respectively) along [100]. Th and As polyhedra are shown in yellow and green, respectively.

symmetry of the $Na_2Th(AsO_4)_2$ crystal structure compared to those of $Cs_2Th(AsO_4)_2$ is due to the rather slight deformation of the Th and As polyhedra and the resulting rearrangement of the Na atom. This is reflected in the geometry of ThO_8 polyhedra as could be seen in Figure 3. For example, the degree of inclination is equal to 90° for the bidentate arsenate anions which are in *trans*-positions in ThO_8 polyhedron within $Cs_2Th(AsO_4)_2$. The same parameter in $Na_2Th(AsO_4)_2$ equals 38°. The crystal structure of $Cs_2Th(AsO_4)_2$ possesses a group of channels along {100} directions occupied by Cs atoms with d(Cs−Cs) = 3.6602(3) Å. It is worth noting that despite the significant difference in the cationic radii, the A—A interatomic distances are still comparable in both crystal structures of $Na_2Th(AsO_4)_2$ and $Cs_2Th(AsO_4)_2$ (3.6061(4) and 3.6602(3) Å for A = Na and Cs, respectively). It can be achieved by arranging Cs atoms in rows within $Cs_2Th(AsO_4)_2$, while Na atoms in $Na_2Th(AsO_4)_2$ are distributed along zigzag chains.

Taking similar synthetic conditions, composition, and nature of outer-sphere cations of the $A_2Th(AsO_4)_2$(A = Li, Na, K, Rb, Cs) series into account, we can assume that the structure formation is driven by the size of alkaline cations. The smallest one (Li) leads to formation of layered structure of $Li_2Th(AsO_4)_2$, which differs significantly from other representatives of this series. The rest of the alkali metal cations show rather similar properties. Nevertheless, the size of the outer sphere cations determines the structural type (i.e., one of the structural types would be adopted only if it contains the cation sites of an appropriate size). The interesting point is that the lowering of symmetry from orthorhombic, in the case of $Na_2Th(AsO_4)_2$, to monoclinic, in the case of $A_2Th(AsO_4)_2$ (A = K, Rb), is followed by a change of the structure type and the subsequent increase of the crystal symmetry in $Cs_2Th(AsO_4)_2$. Despite similarities in a coordination polyhedra topology in the crystal structures of $Na_2Th(AsO_4)_2$ and $Cs_2Th(AsO_4)_2$, higher symmetry of the least one is caused by an exact match of the Cs cation size to the "pore" size for a selected structure type.

Previously a number of compounds with the $A_2T(PO_4)_2$ general formula were reported (for example, $A_3Ce_{1.5}(PO_4)_3 = A_2Ce(PO_4)_2$, where A = Li, Na, K) but only one of them, $Na_2Th(PO_4)_2$, contains thorium.[35,36] The latter compound crystallizes in space group $P2_1/c$ with unit cell parameters a = 7.055(4) Å, b = 21.66(1) Å, c = 9.095(5) Å, and β = 111.56(2)°. In both $Na_2Th(AsO_4)_2$ and $Na_2Th(PO_4)_2$, arsenate and phosphate anions possess the same K[21] coordination type. There are two crystallographically different Th atoms that adopt edge-sharing arsenate-anions in *cis*- and *trans*-configuration in the $Na_2Th(PO_4)_2$ structure. As we mentioned above, for ThO_8 polyhedra in $A_2Th(AsO_4)_2$ (A = Na, K, Rb, and Cs), the edge-sharing arsenate-anions occupy only *trans*- or *cis*-positions. Due to this, the crystal structure of $Na_2Th(PO_4)_2$ could be subdivided into two parts and presented as a combination of the structural units taken from crystal structures of $Na_2Th(AsO_4)_2$ and $K_2Th(AsO_4)_2$. One of these parts contains only Th1 with edge-sharing TO_4 groups located in *trans*-position of ThO_8 polyhedra, part **I.** The second one contains Th2 with edge-sharing TO_4 groups occupying *cis*-positions, part **II**. Figure 4 illustrates the crystal structure of $Na_2Th(PO_4)_2$ built upon continually repeated units **I** and **II**.

3.2. Topological Studies. Topological analysis[37] shows the crystal structures of $A_2Th(AsO_4)_2$ (A = Na, K, Rb, and Cs) based on 3,6-coordinated nets (Figure 5). Classification of these underlying nets with the ADS program of the TOPOS software package reveals a **ant** (anatase) topological type found in the Reticular Chemistry Structure Resource (RCSR).[38] Variation in outer-sphere cation radii and Th atom coordination in the $A_2Th(AsO_4)_2$ (A = Na, K, Rb, Cs) series shows no changes in the topology of these compounds, although the symmetry of the crystal structures varies from monoclinic (A = K and Rb) to tetragonal (A = Cs). The last is identical to **ant** topological type highest symmetry ($I4_1/amd$[38]). Due to similarities of coordination environments in the crystal structure of $Na_2Th(PO_4)_2$ and the titled compounds, the former one is also based on 3,6-coordinated underlying net. Nevertheless, its topology does not coincide with the topology of $A_2Th(AsO_4)_2$ (A = Na, K, Rb, and Cs) and cannot be assigned by TOPOS due to absence of this topological type in its database. In addition, analysis reveals that the underlying net of $Na_2Th(PO_4)_2$ contains four

dx.doi.org/10.1021/ic5018246 | *Inorg. Chem.* 2014, 53, 11231−11241

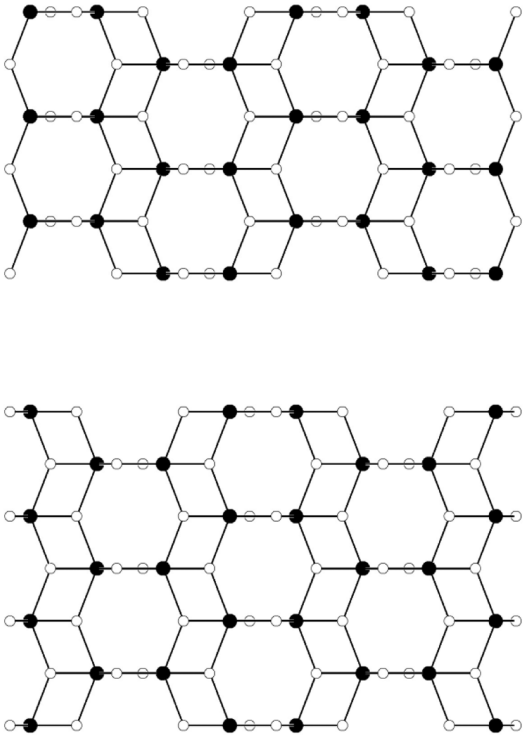

Figure 5. View on underlying net of $Cs_2Th(AsO_4)_2$ (**ant** topological type[38]) along [100] (left) and [010] (right). Black and white sphere corresponds to Th and As atoms, respectively.

independent nodes with different point symbols (**PS**):[39] $4^2.6$, 4^3, $4^5.6^4.8^6$, and $4^5.6^4.8^5.10$, while PS of net nodes of $A_2Th(AsO_4)_2$ (A = Na, K, Rb, Cs) are $4^2.6$ and $4^4.6^2.8^8.10$. This difference reflects the above-discussed fact of the presence of both ThO_8 coordination polyhedra with edge-sharing anions in *cis*- and *trans*-positions. It is not surprising that repetition of the structural units in the crystal structures of $A_2Th(AsO_4)_2$ (A = Na, K) (see above) results in a simpler topology than the topology of their combination in the crystal structure of $Na_2Th(PO_4)_2$. Thus, the nature of oxo-anion centers has an influence on the geometry of the Th coordination polyhedra, as well as on the topology of their crystal structures. The underlying net in $Na_2Th(PO_4)_2$ is more complex because it contains four independent nodes opposite to two in the case of $A_2Th(AsO_4)_2$ (A = Na, K, Rb, Cs).

The topology of $Li_2Th(AsO_4)_2$ is quite different from the above-described one because the structure is two-dimensional. The arsenate anions possess two different coordination types (T^{21} and T^{31}) and each Th atom is surrounded by seven arsenate-anions. Due to this, the crystal structure of $Li_2Th(AsO_4)_2$ is based on a 3,4,7-coordinated net, which is classified by TOPOS as 3,4,7L1 topological type and relates to a square plane net by removing 3-coordinated node.

3.4. Thermal Behavior. The DSC curves $K_2Th(AsO_4)_2$ and $Rb_2Th(AsO_4)_2$ are shown in Figure 6. The DSC curves of $Li_2Th(AsO_4)_2$ as well as $Na_2Th(AsO_4)_2$ show only one strong endothermic peak, which corresponds to the melting point. Melting of $Li_2Th(AsO_4)_2$ and $Na_2Th(AsO_4)_2$ starts at 1324(3) and 1383(3) K, respectively, and is followed by the decomposition of the compounds, which is clearly seen from TG curves due to mass loss. Both direct and reverse thermal measurements for $K_2Th(AsO_4)_2$ and $Rb_2Th(AsO_4)_2$ were carried out up to 1273 K. Despite the fact that these compounds are isostructural, they show different thermal behavior. The heating DSC curve of $K_2Th(AsO_4)_2$ has four prominent endothermal effects with onset temperatures at 1019(3) K, 1069(3) K, 1149(3) K, and 1189(3) K without any change of sample weight, where the first one is very broadened. Cooling DSC curve of $K_2Th(AsO_4)_2$ contains three strong peaks with the onset temperatures of 1144(3) K, 1039(3) K, and 1019(3) K. There is also a minor peak starting at 1184 K. Therefore, all the effects observed in the heating DSC are reversible and show hysteresis of 5−30 K. Both the heating and cooling runs of $Rb_2Th(AsO_4)_2$ DSC curves contain two peaks. The heating data show a strong endothermal peak with an onset temperature of 779(3) K and a moderate peak at 1179(3) K. The respective cooling curve shows a split moderate endothermal peak starting at 1139(3) K and a strong exothermal signal at 669(3) K. As both peaks at 779 and 669 K are similar (excepting sign of thermal effect) on the heating and cooling curves, we will show that they correspond to a reversible phase transition showing a hysteresis of 110 K. The higher hysteresis value in $Rb_2Th(AsO_4)_2$ compared to $K_2Th(AsO_4)_2$ is due to the lower phase transition temperature and, therefore, lower phase transition rate. To study the phase transitions of both $K_2Th(AsO_4)_2$ and $Rb_2Th(AsO_4)_2$ high-temperature powder X-ray diffraction method was employed.

3.5. High-Temperature Powder XRD and Phase Transitions. Samples of $K_2Th(AsO_4)_2$ and $Rb_2Th(AsO_4)_2$ were characterized by means of Rietveld refinements based on the high-temperature X-ray powder diffraction data collected between 300 and 1220 K as given in Figure 7. The metric

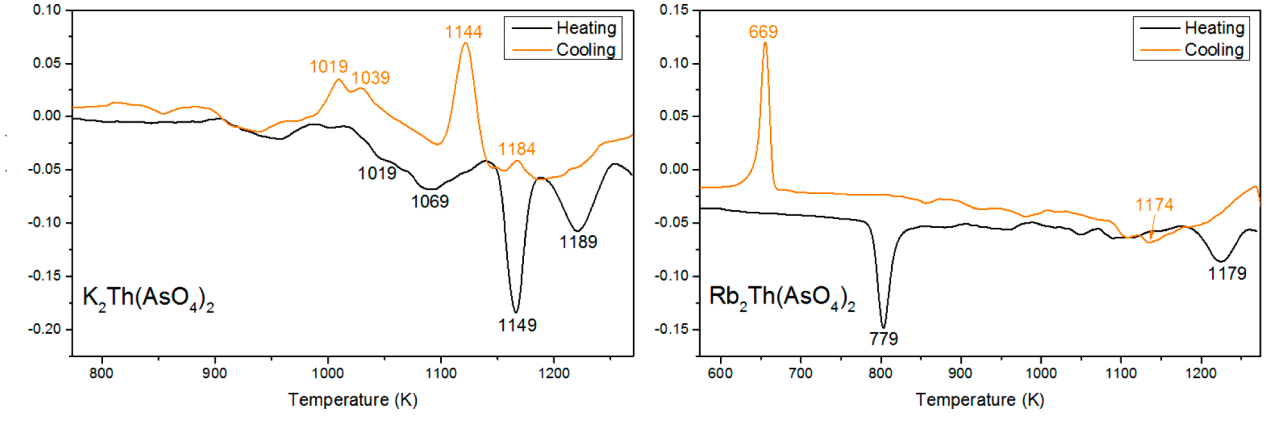

Figure 6. DSC curves of $K_2Th(AsO_4)_2$ and $Rb_2Th(AsO_4)_2$. The peaks are marked with the corresponding onset temperatures.

dx.doi.org/10.1021/ic5018246 | *Inorg. Chem.* 2014, 53, 11231−11241

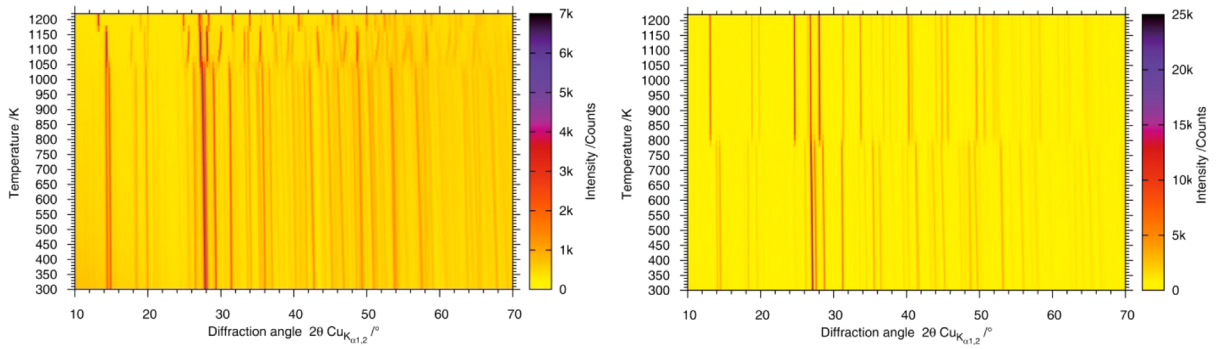

Figure 7. Two-dimensional plot of the temperature-dependent powder pattern of $K_2Th(AsO_4)_2$ (left) and $Rb_2Th(AsO_4)_2$ (right).

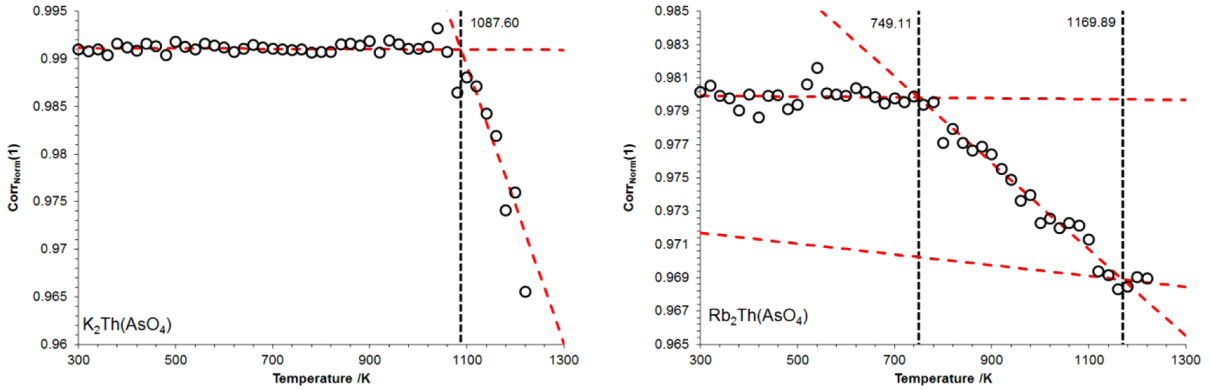

Figure 8. Temperature-dependent development of the autocorrelation parameter of $K_2Th(AsO_4)_2$ (left) and $Rb_2Th(AsO_4)_2$ (right) together with the respective evaluation of transition temperatures.

parameters of both samples were refined for the room-temperature modification of the respective phases as described above until the first phase transition occurred. Although the lattice parameters of the high-temperature phases are similar to the metric of the sodium and cesium compounds the structures could not be refined with isotypic structural models. For $K_2Th(AsO_4)_2$, two phase transitions, first to an orthorhombic and thereafter to a tetragonal metric, are observed, whereas for $Rb_2Th(AsO_4)_2$, a direct phase-transition from the monoclinic metric of the low-temperature phase to a tetragonal one for the high-temperature structure was found.

The temperature-dependent development of the $Corr_{Norm}(1)$ parameter for $K_2Th(AsO_4)$ and $Rb_2Th(AsO_4)$ are shown in Figure 8. For $K_2Th(AsO_4)$, $Corr_{Norm}(1)$ remains constant up to the measurement at 1060 K and decreases linearly with increasing temperature. To establish an onset temperature for the phase transition, regression lines were fitted to both parts and their intersection calculated. By this procedure, 1088 K could be deduced as the onset temperature for the first phase transformation. The $Corr_{Norm}(1)$ parameter for the $Rb_2Th(AsO_4)$ shows an initial constant behavior up to 780 K, although the scattering of the values is generally higher for the Rb-compound than for the potassium compound. In the temperature range from 800 to 1100 K, $Corr_{Norm}(1)$ decreases with a much smaller slope than in the $K_2Th(AsO_4)$ case. The $Corr_{Norm}(1)$ values for temperatures higher than 1100 K could be interpreted as a level-out at a constant value, because the X-ray diffraction patterns do not show any hint for a second change of the compound's structure. Accordingly three linear regressions were chosen to determine the boundary temperatures of the respective ranges by the intersections of the linear regressions. The first phase transition temperature could be determined at 749 K and the temperature at which the high temperature phase is stabilized is 1170 K.

Comparing these temperatures with those obtained from DSC data (Figure 6) of the two compounds, one very prominent signal for the $K_2Th(AsO_4)$ could be found in the DSC signal with an onset temperature of 1149 K. In the case of the $Rb_2Th(AsO_4)$, the DSC signal shows one signal with an onset of 779 K and a weaker one with an onset temperature of 1179 K. The transition temperatures obtained by the autocorrelation analysis are lower than these due to the different heating rates used in both measurements and the additional holding times in the X-ray measurements. In the case of $K_2Th(AsO_4)$, the second phase transition could not be observed in the autocorrelation of the selected range because there is only one observed reflection, which does not change in the course of the transition. Considering other ranges with visible changes due to the second phase transition, the calculated $Corr_{Norm}(1)$ values do not give a clear signal due to the bad definition of the X-ray diffraction data close to the transition temperature.

To obtain intrinsic energy information on the phases, the thermal expansion of solids can be adequately modeled using both Debye quasi-harmonic and Einstein harmonic models. In the Einstein harmonic model, the atoms in a solid are independent oscillators and free from other sources of dynamical entropy. The Debye quasi-harmonic model also assumes independent oscillators, however, with altered frequencies. None of the thermal expansion coefficient (TEC) of the metric parameters saturate at a temperature-independent region for the observed range (Figure 9, inset), which is assumed to be associated with intrinsic anharmonicity leading to anisotropic and anomalous thermal expansion. Because of this observation we carried the first refinements of both phases out using one

dx.doi.org/10.1021/ic5018246 | Inorg. Chem. 2014, 53, 11231−11241

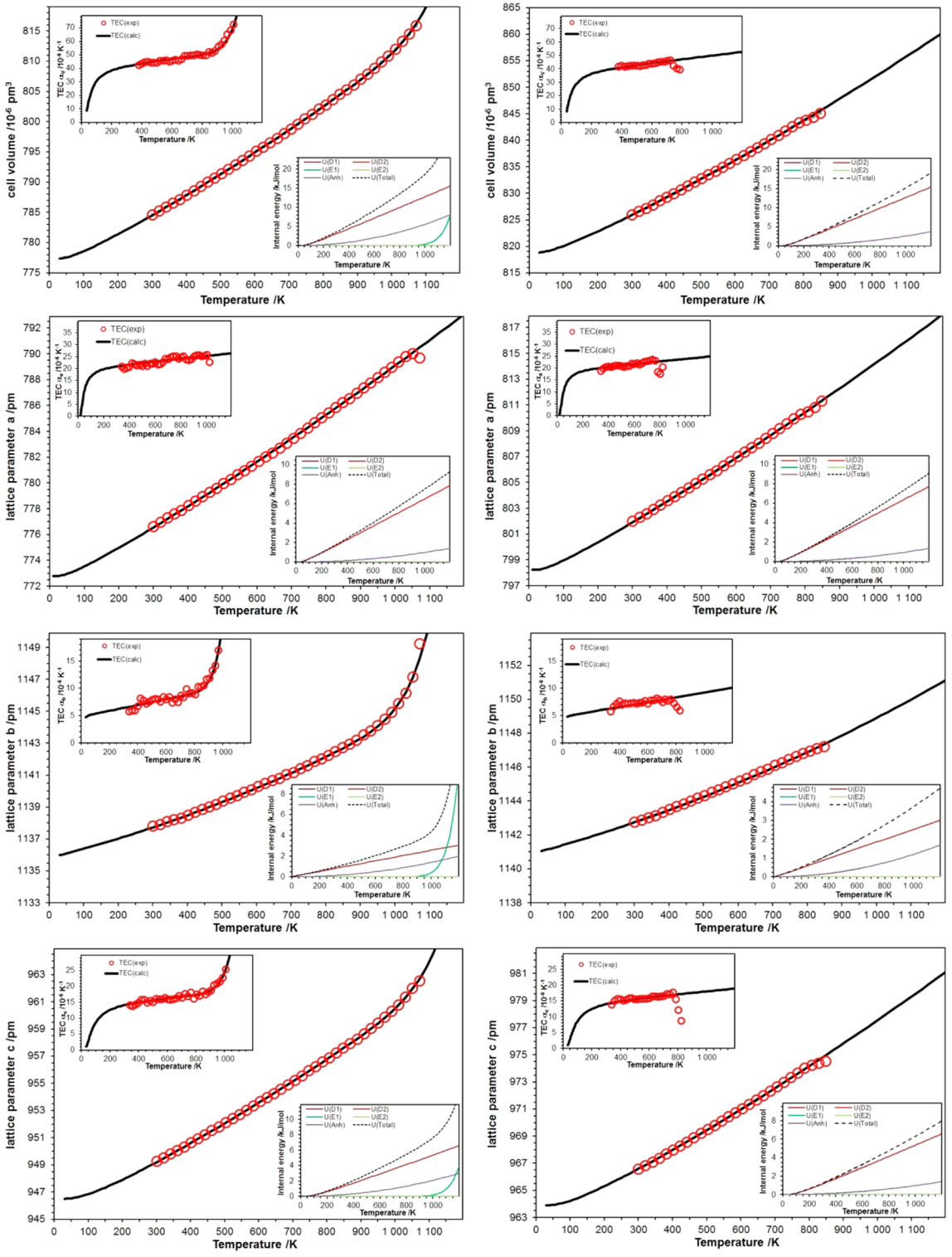

Figure 9. Temperature-dependent metric parameters and thermal expansion coefficients (TEC, inset top) together with the respective DEA fit results and single energy term contribution (insert bottom) for the X-ray powder data of room-temperature phases of $K_2Th(AsO_4)_2$ (left) and $Rb_2Th(AsO_4)_2$ (right).

Debye and the Anharmonicity term ($d = 1$, $e = 0$, k_A) in the general equation:

$$M(T) = M_0 + \sum_{i=1}^{d} k_{Di} U_{Di}(T) + \sum_{i=1}^{e} k_{Ei} U_{Ei}(T) + k_A U_A(T) \quad (1)$$

as given together with further details elsewere.[40] In this equation, $M(T)$ refers to any of the temperature-dependent metric parameters ($V(T)$, $a(T)$, $b(T)$ and $c(T)$); k_{Di}, k_{Ei}, and k_A are adjustable fitting parameters representing thermoelastic information, contributing to Debye (U_{Di}), Einstein (U_{Ei}), and anharmonic (U_A) internal energies, respectively. From these refinements, it could be deduced that the high-temperature behavior of the phases is influenced by the anharmonic phonon behavior whereas the harmonic part could be described nicely

dx.doi.org/10.1021/ic5018246 | Inorg. Chem. 2014, 53, 11231−11241

using quasi-harmonic Debye oscillators. Without data from room-temperature to nearly 0 K, only one Debye term is necessary to describe this phonon/energy contribution.

For the refinement of the thermal behavior of $Rb_2Th(AsO_4)_2$, the Debye-Anharmonicity (DA) model (d = 1, e = 0, k_A) describes the temperature dependency of the all metric parameters as well as the respective thermal expansion coefficient (TEC), as could be seen in Figure 9. Fitted values are given in Table 2. The slight deviations from the calculated curves

Table 2. Values Resulting from the Fitting of the Temperature-Dependent Metric Parameters

metric parameter	V	a	b	c
		$K_2Th(AsO_4)_2$		
model[b]	DEA	DA	DEA	DEA
0 K[a]	777.32	772.78	1135.89	946.52
k_{D1} /10^{-14}	1400.61	698.10	253.56	613.88
θ_{D1} /K	223.53	177.35	24.83	336.51
k_{E1} /10^{-14}	2.4×10^8	-	8.0×10^8	1.7×10^8
θ_{E1} /K	18653	-	19826	19091
k_A /10^{-12}	−518.72	−200.38	−280.49	−193.48
		$Rb_2Th(AsO_4)_2$		
model[b]	DA	DA	DA	DA
0 K[a]	818.84	798.22	1140.92	963.90
k_{D1} /10^{-14}	1387.83	684.81	252.95	613.88
θ_{D1} /K	225.73	177.69	24.12	336.51
k_{E1} /10^{-14}	-	-	-	-
θ_{E1} /K	-	-	-	-
k_A /10^{-12}	−511.49	−191.71	−237.63	−195.58

[a]Cell parameters a, b, c and cell volume V at 0 K given in pm and 10^6pm^3, respectively, with errors estimated from the calculations to 5%. [b]DA = single Debye Anharmonic model, DEA = single Debye single Einstein Anharmonic model, $\theta_A = \theta_{D1}$.

at high temperatures represent the beginning phase transition. In this respect, the thermal behavior of $Rb_2Th(AsO_4)_2$ could be compared with the chemically similar $Rb_2Th(MoO_4)_3$ phase.[41] However, whereas for $Rb_2Th(MoO_4)_3$ a displacive phase transition was assumed, a clear observation of a phase transition for $Rb_2Th(AsO_4)_2$ could be reported here. Because the X-ray powder pattern are similar before and after the heating measurements, a displacive phase transition is very likely.

In $K_2Th(AsO_4)_2$, only the a lattice parameter behaves like the isotypic $Rb_2Th(AsO_4)_2$ compound while heating and could also be described using a DA model. The Debye contribution is nearly the same (Table 2), showing only a 15 K higher Debye temperature of the potassium compound than the rubidium one. This correlates with a ∼ 5% higher thermoelastic constant for the anharmonicity contribution. The deviations of the proposed lattice parameters at 0 K are due to different cation sizes. For the b and c lattice parameter and consequently because no negative thermal expansion was observed and for the unit cell volume there is only a DEA fitting using one Debye, one Einstein and the anharmonicity term (d = 1, e = 1, $k_A \neq 0$) lead to reasonable fits of the metric parameter developments as well as the thermal expansion coefficients. But also in this case k_{D1}, θ_{D1}, and k_A were found to show comparable values for $K_2Th(AsO_4)_2$ and $Rb_2Th(AsO_4)_2$ (Table 2). A strong increase of the metric parameters and, as a consequence, a strong TEC increase have to be modeled by the respective Einstein contributions. This strong increase of the b lattice parameter in $K_2Th(AsO_4)_2$ is comparable to the strong temperature-dependent increase of the cubic a lattice parameter found for the tricritical displacive phase transition of nitrate-sodalites,[42] hence, is also explained in this case as indicator for a phase transition with a second-order/tricritical phase transition. Further investigations searching for the order parameter of the respective phase transition must confirm a bigger change of the order parameter during the monoclinic−orthorhombic phase transition in $K_2Th(AsO_4)_2$ and a less pronounced behavior or different mechanism for the monoclinic−tetragonal phase transition in $Rb_2Th(AsO_4)_2$ to understand the different expansion behavior close to and around the phase transition temperature.

3.3. Raman and IR Spectra. The Raman spectra of $A_2Th(AsO_4)_2$ (A = Li, Na, K, Rb, Cs) are presented in Figure 10.

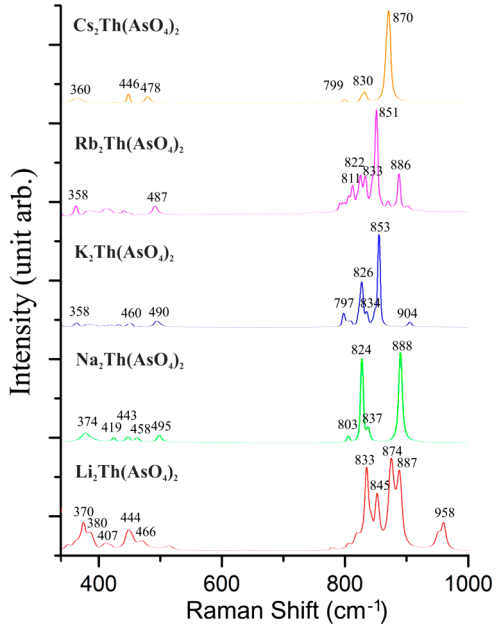

Figure 10. Raman spectra of $A_2Th(AsO_4)_2$ (A = Li, Na, K, Rb, Cs).

The spectra could be divided into low- and high-frequency parts with the ranges of 200−550 cm^{-1} and 798−958 cm^{-1}. According to literature data,[43−47] the low-frequency part corresponds to symmetric bending (υ_2) and out-of-plane bending (υ_4) modes, whereas high-frequency region corresponds to symmetric (υ_1) and antisymmetric (υ_3) stretching vibrations. The band wavenumbers and their assignments are given in Table 3. The general tendency of the spectra is that the frequency of the most intensive bands (874, 888, 853, 851, and 870 cm^{-1} for A = Li, Na, K, Rb, and Cs, respectively) is in an inverted correlation with the average As−O bond distances (1.685, 1.680, 1.685, 1.689, and 1.681 Å, respectively).

Same as Raman, IR spectra of the compounds consist of two parts: a high-wavelength region with a range of 700 cm^{-1} − 1000 cm^{-1} and low-wavelength region with a range of 400−600 cm^{-1} (Figure S1 in Supporting Information). The high-wavelength region corresponds to the stretching vibrations, whereas the low-wavelength region corresponds to the bending ones.

It is noteworthy that the amount and intensity of peaks in the spectra of the studied compounds correlate with the symmetry of their structures. Arsenic atoms in the structure of the most symmetric $Cs_2Th(AsO_4)_2$ have C_{2v} site-symmetry, and each Raman and IR spectra of this compound contains only one very intensive peak (Figure 10 and Figure S1 in Supporting Information).

dx.doi.org/10.1021/ic5018246 | Inorg. Chem. 2014, 53, 11231−11241

Table 3. Assignment of Selected Raman Bands Corresponding to AsO_4 Vibrational Modes

	this study/cm^{-1}	ref data/cm^{-1}	assignment[a]	ref
$Li_2Th(AsO_4)_2$	958		not assigned	
	887	884	υ_1 and υ_3	43
	874	877		44
	845	849		44
	833	832		44
	466	467	υ_4	45
	444	446		44
	407	398		44
	380	382		44
	370	368		44
$Na_2Th(AsO_4)_2$	888	884	υ_1 and υ_3	44
	837	832		46
	824	823		44
	803	808		44
	495	496	υ_4	44
	458	460		44
	443	446		44
	419	416		44
	374	377		45
$K_2Th(AsO_4)_2$	904	905	υ_1 and υ_3	45
	853	853		46
	834	832		44
	826	823		44
	797	798		47
	490	496	υ_2 and υ_4	44
	460	460		44
	358	360		44
$Rb_2Th(AsO_4)_2$	886	884	υ_1 and υ_3	44
	851	853		45
	833	832		44
	822	822		44
	813	815		44
	487	482	υ_2 and υ_4	44
	358	360		44
$Cs_2Th(AsO_4)_2$	870	873	υ_1 and υ_3	46
	830	832		44
	799	797		45
	478	478	υ_2 and υ_4	44
	446	446		44
	360	360		44

[a] υ_1 – symmetric stretching vibrations; υ_2 – symmetric bending vibrations; υ_3 – antisymmetric stretching vibrations; υ_4 – out-of-plane bending vibrations.

The less symmetric structure of $Na_2Th(AsO_4)_2$ (site-symmetry of the As atoms is C_2) causes an increase of amount of intensive peaks up to two in the Raman and up to three in the IR spectrum. Further symmetry reduction of the crystal structures is accompanied by additional splitting of the peaks in the cases of $Li_2Th(AsO_4)_2$, $K_2Th(AsO_4)_2$, and $Rb_2Th(AsO_4)_2$, which structures contain As atoms in the positions with C_1 site-symmetry.

4. CONCLUSIONS

A high-temperature solid-state reaction method was employed to obtain single crystals and pure powder samples of five novel thorium arsenate compounds with the general formula $A_2Th(AsO_4)_2$ (A = Li, Na, K, Rb, Cs). Despite the same stoichiometry, the crystal structures and thermal/spectroscopic properties of these compounds are significantly influenced by the size of the outer-sphere alkali cations. The crystal structure of the Li-containing compound is 2D, while those of other compounds are 3D. In the structures of $A_2Th(AsO_4)_2$ (A= Na, K, Rb, Cs), arsenate anions are tetradentate, adopt a K^{21} coordination type, and the Th atoms are 8-fold coordinated. The same coordination modes of the AsO_4 groups and coordination numbers of the Th atoms lead to a common underlying net with **ant** topological type for these compounds. The symmetry of the structures varies from monoclinic to tetragonal and relates to the environment of the Th atoms. In orthorhombic $Na_2Th(AsO_4)_2$ and tetragonal $Cs_2Th(AsO_4)_2$, the Th atoms coordinate edge-sharing arsenate anions in *trans*-positions, while in isotypic monoclinic $K_2Th(AsO_4)_2$ and $Rb_2Th(AsO_4)_2$, they coordinate in *cis*-positions. The difference in symmetry between $Na_2Th(AsO_4)_2$ and $Cs_2Th(AsO_4)_2$ is due to a variation of outer-sphere cation size, though motifs of these structures are similar.

The difference in size of K and Rb cations has no significant influence on the room-temperature crystal structures of $K_2Th(AsO_4)_2$ and $Rb_2Th(AsO_4)_2$ because both compounds are isotypic. Nevertheless, the thermal behavior of these compounds is defined by the nature of the outer-sphere cations. Two temperature-induced phase transitions were found in both $K_2Th(AsO_4)_2$ and $Rb_2Th(AsO_4)_2$ by means of high-temperature powder XRD accompanied by DSC in a range of 300−1220 K. The structure of $K_2Th(AsO_4)_2$ changes twice upon heating, first from a monoclinic to an orthorhombic metric at 1088 K and therefore to a tetragonal one in a range of 1150−1200 K. One phase transition in $Rb_2Th(AsO_4)_2$ at 749 K is followed by a direct monoclinic-tetragonal metric transformation, whereas another one at 1170 K is not related to any structural change but to the stabilization of high-temperature phase. Despite the fact that metrics of the high-temperature modifications of $K_2Th(AsO_4)_2$ and $Rb_2Th(AsO_4)_2$ are similar to the corresponding metrics of the room-temperature modifications of orthorhombic $Na_2Th(AsO_4)_2$ and tetragonal $Cs_2Th(AsO_4)_2$, the single crystal structures of the least two does not fit high-temperature diffraction patterns of $K_2Th(AsO_4)_2$ and $Rb_2Th(AsO_4)_2$.

■ ASSOCIATED CONTENT

Supporting Information

This includes compound structures in cif format, IR spectra, powder XRD patterns, and results of EDX analysis. This material is available free of charge via the Internet at http://pubs.acs.org.

■ AUTHOR INFORMATION

Corresponding Author

*E-mail: e.alekseev@fz-juelich.de.

Notes

The authors declare no competing financial interest.

■ ACKNOWLEDGMENTS

The authors are grateful for Hartmut Schlenz (IEK-6, Forschungszentrum Jülich) for his kind help in Raman spectra collection. E.V.A. is grateful for the Helmholtz Association for funding within VH-NG-815 project and to the Federal Ministry of Education and Research (BMBF) for its support (Support Code 02NUK021A). T.M.G. thanks the Deutsche Forschungsgemeinschaft (DFG) for the financial support in the Heisenberg Programme (GE1981/3-1 and GE1981/3-2).

REFERENCES

(1) MacDonald, M. R.; Fieser, M. E.; Bates, J. E.; Ziller, J. W.; Furche, F.; Evans, W. J. *J. Am. Chem. Soc.* **2013**, *135*, 13310−13313.
(2) Katz, J. J.; Morss, L. R.; Seaborg, G. T. *The Chemistry of the Actinide and Transactinide Elements: volumes 1−6*; Springer Science+Business Media B.V: Dordrecht, 2011.
(3) Tananaev, I. G.; Nikonov, M. V.; Myasoedov, B. F.; Clark, D. L. *Journal of Alloys and Compounds* **2007**, *444−445*, 668−672.
(4) Villa, E. M.; Marr, C. J.; Jouffret, L. J.; Alekseev, E. V.; Depmeier, W.; Albrecht-Schmitt, T. E. *Inorg. Chem.* **2012**, *51*, 6548−6558.
(5) Villa, E. M.; Marr, C. J.; Diwu, J.; Alekseev, E. V.; Depmeier, W.; Albrecht-Schmitt, T. E. *Inorg. Chem.* **2013**, *52*, 965−973.
(6) Yeon, J.; Smith, M. D.; Tapp, J.; Möller, A.; zur Loye, H.-C. *J. Am. Chem. Soc.* **2014**, *136*, 3955−3963.
(7) Raison, P.; Jardin, R.; Bouëxière, D.; Konings, R. M.; Geisler, T.; Pavel, C.; Rebizant, J.; Popa, K. *Phys. Chem. Miner.* **2008**, *35*, 603−609.
(8) Wallez, G.; Bregiroux, D.; Popa, K.; Raison, P. E.; Apostolidis, C.; Lindqvist-Reis, P.; Konings, R. J. M.; Popa, A. F. *Eur. J. Inorg. Chem.* **2011**, *2011*, 110−115.
(9) Villa, E. M.; Wang, S.; Alekseev, E. V.; Depmeier, W.; Albrecht-Schmitt, T. E. *Eur. J. Inorg. Chem.* **2011**, *2011*, 3749−3754.
(10) Brandel, V.; Dacheux, N. *J. Solid State Chem.* **2004**, *177*, 4755−4767.
(11) Bénard, P.; Brandel, V.; Dacheux, N.; Jaulmes, S.; Launay, S.; Lindecker, C.; Genet, M.; Louër, D.; Quarton, M. *Chem. Mater.* **1996**, *8*, 181−188.
(12) Dacheux, N.; Podor, R.; Chassigneux, B.; Brandel, V.; Genet, M. *J. Alloys Compd.* **1998**, *271−273*, 236−239.
(13) Dacheux, N.; Clavier, N.; Wallez, G.; Brandel, V.; Emery, J.; Quarton, M.; Genet, M. *Mater. Res. Bull.* **2005**, *40*, 2225−2242.
(14) Dacheux, N.; Podor, R.; Brandel, V.; Genet, M. *J. Nucl. Mater.* **1998**, *252*, 179−186.
(15) Dacheux, N.; Thomas, A. C.; Brandel, V.; Genet, M. *J. Nucl. Mater.* **1998**, *257*, 108−117.
(16) Deifel, N. P.; Holman, K. T.; Cahill, C. L. *Chem. Commun.* **2008**, 6037−6038.
(17) Renard, C.; Obbade, S.; Abraham, F. *J. Solid State Chem.* **2009**, *182*, 1377−1386.
(18) Alekseev, E. V.; Krivovichev, S. V.; Malcherek, T.; Depmeier, W. *J. Solid State Chem.* **2008**, *181*, 3010−3015.
(19) Wylie, E. M.; Dawes, C. M.; Burns, P. C. *J. Solid State Chem.* **2012**, *196*, 482−488.
(20) Salvadó, M. A.; Pertierra, P.; Bortun, A. I.; Trobajo, C.; García, J. R. *Inorg. Chem.* **2008**, *47*, 7207−7210.
(21) Wallez, G.; Raison, P. E.; Dacheux, N.; Clavier, N.; Bykov, D.; Delevoye, L.; Popa, K.; Bregiroux, D.; Fitch, A. N.; Konings, R. J. M. *Inorg. Chem.* **2012**, *51*, 4314−4322.
(22) Dacheux, N.; Clavier, N.; Wallez, G.; Quarton, M. *Solid State Sci.* **2007**, *9*, 619−627.
(23) Kalinin, V. B.; Golubev, A. M.; Tafeenko, V. A.; Stefanovich, S. Y. *Sov. Phys. Crystallogr.* **1992**, *37*, 1220−1226.
(24) Matković, B.; Kojić-Prodić, B.; Šlijukić, M.; Topić, M.; Willett, R. D.; Pullen, F. *Inorg. Chim. Acta* **1970**, *4*, 571−576.
(25) Matković, B.; Prodic, B.; Šlijukić, M. *Croat. Chim. Acta* **1968**, *40*, 147−161.
(26) Krishnan, K.; Sali, S. K.; Singh Mudher, K. D. *J. Alloys Compd.* **2006**, *414*, 310−316.
(27) Alekseev, E. V.; Krivovichev, S. V.; Depmeier, W. *J. Solid State Chem.* **2009**, *182*, 2977−2984.
(28) Sheldrick, G. M. *Acta Crystallogr. A* **2007**, *64*, 112−122.
(29) Farrugia, L. J. *J. Appl. Crystallogr.* **2012**, *45*, 849−854.
(30) Blatov, V. A.; Serezhkin, V. N. *Russ. J. Inorg. Chem.* **2000**, *45*, S105−S222.
(31) Blatov, V. A.; Shevchenko, A. P.; Serezhkin, V. N. *J. Appl. Crystallogr.* **2000**, *33*, 1193−1193.
(32) Butz, T. *Fouriertransformationen für Fußgänger*, 5th ed.; Springer-Verlag: Wiesbaden, Germany, 2007.
(33) Serezhkin, V. N.; Vologzhanina, A. V.; Serezhkina, L. B.; Smirnova, E. S.; Grachova, E. V.; Ostrova, P. V.; Antipin, M. Y. *Acta Crystallogr. B* **2009**, *65*, 45−53.
(34) Vologzhanina, A. V.; Serezhkina, L. B.; Neklyudova, N. A.; Serezhkin, V. N. *Inorg. Chim. Acta* **2009**, *362*, 4921−4925.
(35) Galesic, N.; Matković, B.; Topić, M.; Coffou, E.; Šlijukić, M. *Croat. Chim. Acta* **1984**, *57*, 597.
(36) Orlova, A. I.; Kitaev, D. B.; Kazantsev, N. G.; Samoilov, S. G.; Kurazhkovskaya, V. S.; Vopilina, E. N. *Radiochemistry* **2002**, *44*, 326−331.
(37) Alexandrov, E. V.; Blatov, V. A.; Kochetkov, A. V.; Proserpio, D. M. *CrystEngComm* **2011**, *13*, 3947.
(38) O'Keeffe, M.; Peskov, M. A.; Ramsden, S. J.; Yaghi, O. M. *Acc. Chem. Res.* **2008**, *41*, 1782−1789.
(39) Blatov, V. A.; O'Keeffe, M.; Proserpio, D. M. *CrystEngComm* **2010**, *12*, 44.
(40) Murshed, M. M.; Gesing, T. M. *Mater. Res. Bull.* **2013**, *48*, 3284−3291.
(41) Xiao, B.; Gesing, T. M.; Kegler, P.; Modolo, G.; Bosbach, D.; Schlenz, H.; Suleimanov, E. V.; Alekseev, E. V. *Inorg. Chem.* **2014**, *53*, 3088−3098.
(42) Rüscher, C. H.; Gesing, T. M.; Buhl, J.-C. *Z. Für Krist.* **2003**, *218*, 332−344.
(43) Frost, R. L.; Martens, W. N.; Williams, P. A. *J. Raman Spectrosc.* **2002**, *33*, 475−484.
(44) Frost, R. L.; Martens, W.; Williams, P. A.; Kloprogge, J. T. *J. Raman Spectrosc.* **2003**, *34*, 751−759.
(45) Martens, W.; Frost, R. L.; Kloprogge, J. T. *J. Raman Spectrosc.* **2003**, *34*, 90−95.
(46) Frost, R. L.; Kloprogge, J. T. *Spectrochim. Acta, Part A* **2003**, *59*, 2797−2804.
(47) Paques-Ledent, M. T.; Tarte, P. *Spectrochim. Acta, Part A* **1974**, *30*, 673−689.